ChemComm

Accepted Manuscript

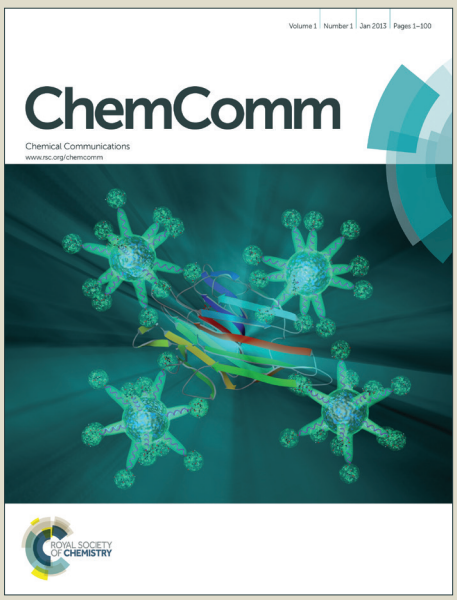

ROYAL SOCIETY OF CHEMISTRY

www.rsc.org/chemcomm

ChemComm

COMMUNICATION

Single Nanoparticle-based Sensor for Hydrogen Peroxide (H_2O_2) via Cytochrome *c*-mediated Plasmon Resonance Energy Transfer†

Received 00th January 20xx,
Accepted 00th January 20xx

DOI: 10.1039/x0xx00000x

www.rsc.org/chemcomm

Yura Kim,[‡a] Ji Youn Park,[‡a] Hye Young Kim,[a] Minzae Lee,[b] Jongheop Yi[b] and Inhee Choi[*a]

Herein, we report a novel method for H_2O_2 detection based on a single plasmonic nanoprobe via cytochrome *c* (Cyt *c*)-mediated plasmon resonance energy transfer (PRET). Dynamic spectral changes were observed in the fingerprint quenching dip of a single plasmonic nanoprobe in response to changes in the redox state of Cyt *c*, induced by H_2O_2. Based on changes in the spectral profile of the single plasmonic nanoprobe, H_2O_2 was successfully detected in the wide concentration range from 100 mM to 10 nM, including physiologically relevant micromolar and nanomolar concentration.

Reactive oxygen species (ROS) are natural byproducts that are frequently generated through cellular metabolism.[1] Hydrogen peroxide (H_2O_2) is one of the major ROS, and plays a critical role in normal physiological processes as well as disease mechanisms.[2, 3] For example, H_2O_2 is deeply associated with intracellular signaling pathways, such as apoptosis and proliferation,[1, 4] as described in Fig. S1, ESI†. Since H_2O_2 acts as an oxidizing agent owing to its strong electronegativity, it is reported that high levels of *in vivo* concentrations of H_2O_2 induce cellular damage (i.e., oxidation of DNA, lipids, and proteins).[1, 4-8] In case of low levels H_2O_2, it can influence proliferation.[9, 10] Due to these adverse implications in disease pathology, particularly oxidative stress in neurological disorders[6] and cancers,[2, 3] techniques for monitoring the generation of H_2O_2 have gained focus. A variety of H_2O_2 detection methods have been developed. These include optical techniques (i.e., based on fluorescence,[11-13] luminescence,[14, 15] and absorbance[16, 17]) and electrochemical techniques combined with enzymes[18, 19] or non-enzymatic electrodes such as a redox active materials (i.e., metal nanoparticles).[20, 21] Moreover, conventional titrimetry[22] is time-consuming and is not sufficiently sensitive for detection of low levels of H_2O_2. Gasometry[23] is also inappropriate for detecting H_2O_2 at low concentrations and is sensitive to humidity and temperature. Enzymatic electrochemical techniques suffer from poor reproducibility and stability due to denaturation of the enzymes at certain temperatures and pH.[24, 25] Optical methods are occasionally hampered by issues of low selectivity and sensitivity due to interferences from other species such as metal ions or degradation of the probe.[26, 27] In particular, fluorescence techniques usually have low selectivity or sensitivity due to autoxidation of the fluorophores by light[2] or photobleaching by H_2O_2.[27] In order to overcome these limitations, more efficient detection methods that allow for enhanced sensitivity, reproducibility, selectivity, stability, and further *in vivo* applicability have been actively sought.

Herein, we present a new method for sensitive and selective detection of H_2O_2 using a single nanoparticle and cytochrome *c* (Cyt *c*)-mediated plasmon resonance energy transfer (PRET). The single nanoparticles used as sensing probes in the present approach offer the advantages of biocompatibility, photostability, and excellent optical properties such as an enhanced scattering.[28, 29]

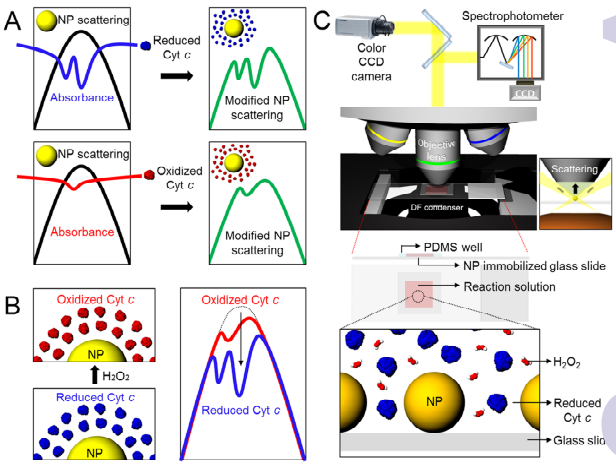

Fig. 1 Novel method for H_2O_2 detection using a single nanoparticle and Cyt *c*-mediated plasmon resonance energy transfer. (A) Illustration of quenching dip in Rayleigh scattering spectrum of a single nanoparticle induced by plasmon resonance energy transfer from the nanoparticle to Cyt *c*. (B) Scheme showing dynamic spectral change in the fingerprint quenching dip of a single nanoparticle based on changes in the redox state of Cyt *c* induced by H_2O_2. (C) Configurations of a dark-field microscopy combined with a spectrophotometer and a sensor chip for collecting single nanoparticle spectra upon exposure to H_2O_2.

[a] *Nanobiointerface Laboratory, Department of Life science, University of Seoul, Dongdaemun-ku, Seoul 130-743, Republic of Korea.*
[b] *Department of Chemical and Biological Engineering, Seoul National University, Gwanak-ku, Seoul 151-742, Republic of Korea.*
† Electronic Supplementary Information (ESI) available: [details of any supplementary information available should be included here]. See DOI: 10.1039/x0xx00000x

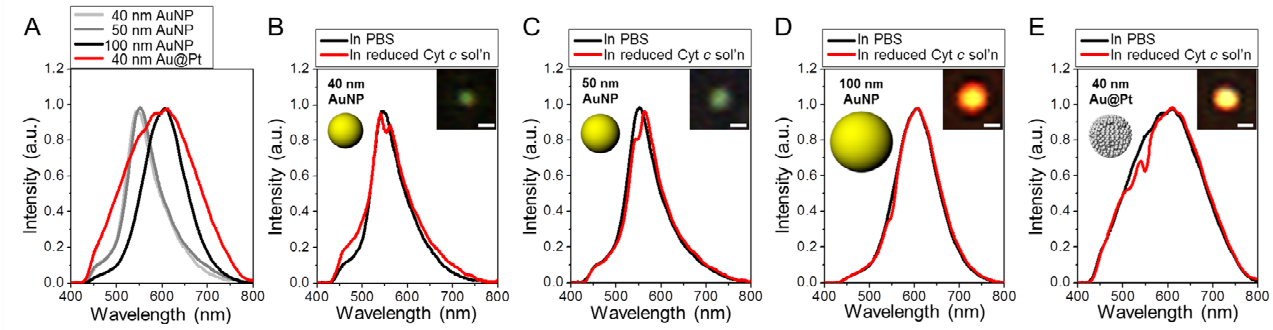

Fig. 2 Selection of optimal sensing probe. (A) Rayleigh scattering spectra of 40, 50 and 100 nm AuNP, and 40 nm Au@Pt in PBS. (B-E) Changes in Rayleigh scattering spectra of 40, 50 and 100 nm AuNP, and 40 nm Au@Pt in reduced Cyt *c* solution. Unique spectral quenching dips are observed in the reduced Cyt *c* solution. The scale bars for dark-field image are 2 μm.

In addition, Cyt *c* is a representative redox active metalloprotein that possesses a heme structure as an active site,[30, 31] where heme participates in electron transport in the cellular system.[30, 32] For example, in the presence of oxidants (i.e., H_2O_2), ferrous iron (Fe^{2+}) in the heme of Cyt *c* is oxidized to ferric iron (Fe^{3+}).[33-36] Interestingly, the absorption spectra of reduced Cyt *c* and oxidized Cyt *c* are clearly distinct (Fig. 1A). Notably, reduced Cyt *c* has absorption peaks around 550 nm and 525 nm, whereas oxidized Cyt *c* has an absorption peak around 530 nm.[37] The sensing principle employed herein is based on the recently reported PRET phenomenon.[37-39] In this system, Cyt *c* in close proximity to the nanoparticle absorbs Rayleigh scattering from the nanoparticle, which results in the distinct spectral quenching dip in accordance with the redox state of Cyt *c*.[37, 39, 40] Accordingly, H_2O_2-induced oxidation of reduced Cyt *c*[36, 41] gives rise to a change in the spectral quenching dip,[40] which functions as a sensing signal (Fig. 1B).

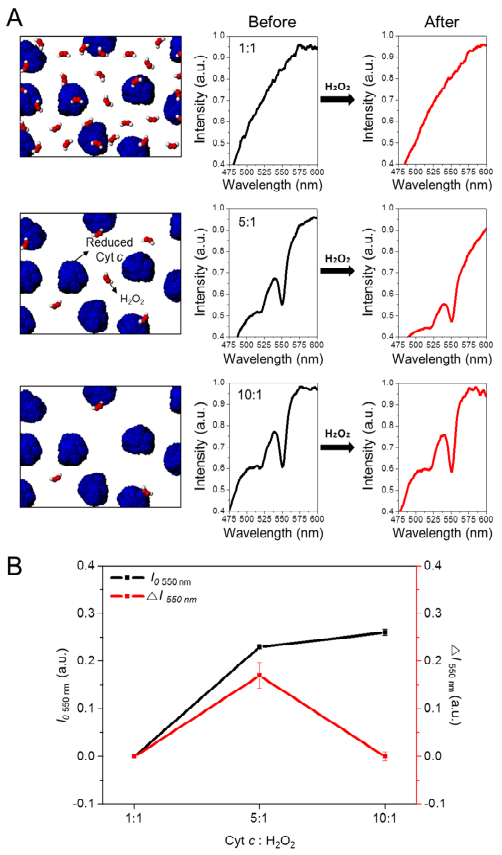

Fig. 3 Determination of optimal reaction conditions for H_2O_2 detection. (A) Changes in the spectral quenching dip induced by H_2O_2 with respect to the relative ratio of Cyt *c*. (B) Plot of initial quenching dip ($I_{0\ 550\ nm}$) and change of quenching dip ($\triangle I_{550\ nm}$) with respect to the relative ratio of Cyt *c*.

In order to find an optimal nanoparticle probe, 40 nm, 50 nm and 100 nm Au nanoparticles (AuNPs) and a core-shell nanoparticle comprising a 40 nm Au core and 4 nm Pt satellites (40 nm Au@Pt) which have plasmon bands around the absorption bands of Cyt *c* were tested. 40 nm Au@Pt nanoparticles were synthesized by the previously reported protocol[42] (see supplementary method) and characterized with high angle annular dark field scanning transmission electron microscopy (HAADF-STEM) analysis and elemental mapping obtained from energy-dispersive X-ray spectrometry (EDX) (Fig. S2 in ESI†). Sensor chips were prepared by immobilization of the nanoparticles on glass slides that were premodified with 3-aminopropyltriethoxysilane (APTES) and trimethoxyoctadecylsilane (TMOS). In order to confine a reaction solution, an elastomeric well prepared with polydimethylsiloxane (PDMS) was placed on the nanoparticle immobilized glass slide (see Fig. 1C and Fig. S3, ESI†). Using dark-field nanospectroscopy (i.e., dark-field microscopy combined with a spectrophotometer shown in Fig. 1C),[28, 43] scattering spectra of individual nanoparticles on the glass slide were characterized. As shown in Fig. 2A, the scattering spectra of the 40 nm, 50 nm and 100 nm AuNPs are characterized by narrow plasmon bands, whereas a broad band is observed in the case of 40 nm Au@Pt. The broadening of the scattering band can be attributed to Pt particles decorated onto the surface of the Au core nanoparticle.[42, 44] Reduced Cyt *c* was prepared by 12 h incubation of native Cyt *c* with ascorbic acid (AA), followed by exposure to the nanoparticle-immobilized sensor chip. The most striking quenching dips for reduced Cyt *c* around 525 nm and 550 nm were observed with the use of 40 nm Au@Pt due to its broad plasmon band, whereas the 40 nm, 50 nm and 100 nm AuNPs gave rise to a single quenching dip (Fig. 2B-2E) around 550 nm. Based on these observations, 40 nm Au@Pt was selected as a sensing probe for further detection of H_2O_2.

To determine the optimal reaction conditions for H_2O_2 detection, the reagent to analyte ratio (i.e., Cyt *c*:H_2O_2) was examined. The concentration of Cyt *c* (as a reagent) was fixed to 100 µM based on previous studies.[45] Increasing the amount of 100 µM Cyt *c* caused an

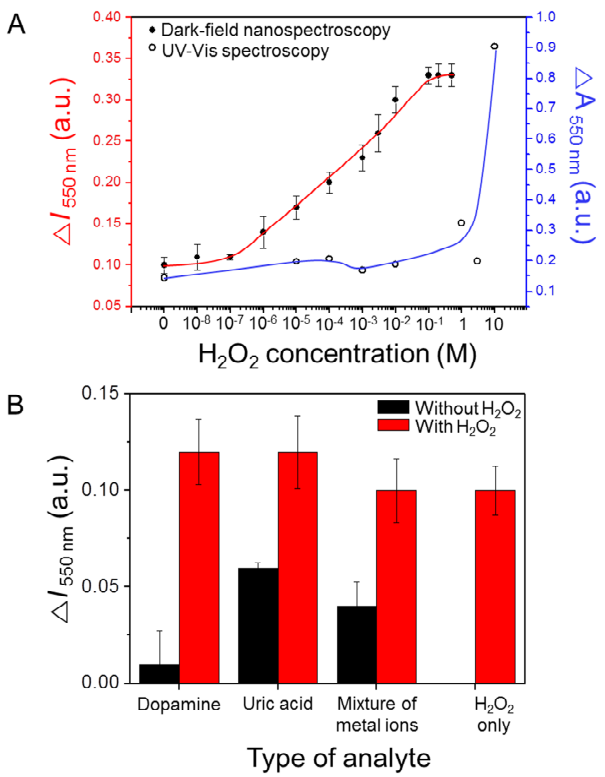

Fig. 4 Sensitive and selective detection of H_2O_2 using a single nanoparticle. (A) Sensitivity test: linear range for single nanoparticle based detection (i.e., dark-field nanospectroscopy) was compared with ensemble-averaged detection (i.e., UV-Vis spectroscopy). Single nanoparticle based detection showed a linear relationship over a wide concentration range from 100 nM to 100 mM, which was much lower than that of the UV-Vis spectroscopic technique. (B) Selectivity test: 11 biologically relevant metal ions (i.e., Co^{2+}, K^+, Fe^{3+}, Ca^{2+}, Pb^{2+}, Fe^{2+}, Mg^{2+}, Ni^{2+}, Mn^{2+}, Zn^{2+}, and Cd^{2+}) or small molecules (i.e., dopamine and uric acid) were tested at an equimolar (100 μM) concentration. When H_2O_2 was present in the analyte solutions, signal change was comparable to that obtained with H_2O_2 only (red bars). While, minimal changes were observed in the case of absence of H_2O_2 (black bars).

increase of the initial quenching dip ($I_{0\ 550\ nm}$) of the probe (Fig. 3B). The change in the quenching dip after exposure to H_2O_2 ($\Delta I_{550\ nm}$) was highest at the middle ratio (5:1). Fig. 3A shows that at the low 1:1 Cyt *c*:H_2O_2 ratio, no quenching dip ($I_{0\ 550\ nm} \approx 0$) was observed for the initial probe due to the small amount of Cyt *c*, and consequently no significant signal was detected after adding H_2O_2 (i.e., $\Delta I_{550\ nm} \approx 0$). In the presence of a large amount of Cyt *c* (10:1), $I_{0\ 550\ nm}$ was relatively high; however, $\Delta I_{550\ nm}$ changed marginally even after exposure to 1 mM H_2O_2. Based on these results, a 5:1 ratio of Cyt *c* to H_2O_2 was selected for the ensuing experiments. Different AA concentrations (10 mM, 50 mM, and 100 mM) were also evaluated to find the optimum conditions for Cyt *c* reduction; 50 mM AA was selected since this produced the highest $\Delta I_{550\ nm}$ value upon exposure to H_2O_2 (Fig. S4, ESI†).

Having selected the optimal probe and reaction conditions for H_2O_2 detection, a sensitivity test was carried out with the developed single 40 nm Au@Pt probe using dark-field nanospectroscopy and the results were compared with those from the conventional UV-Vis spectroscopy (i.e., ensemble-averaged detection method). Various concentrations of H_2O_2 including physiologically relevant micromolar to nanomolar concentration[1] were tested. As shown in Fig. 4A, the single nanoparticle based detection showed a linear relationship over a wide concentration range from 100 nM to 100 mM. At a higher concentration of H_2O_2 (i.e., 1 M), the quenching dip disappeared entirely (Fig. S5, ESI†). The detection limit of the developed method was 10 nM, which is much lower than that of the UV-Vis spectroscopic technique (around 1 M, see Fig. S6, ESI†). Fig. 4B also shows the selectivity of the proposed method for H_2O_2 among biologically relevant metal ions and small molecules. The mixture solutions used for the selectivity test were prepared with 11 metal ions (i.e., Co^{2+}, K^+, Fe^{3+}, Ca^{2+}, Pb^{2+}, Fe^{2+}, Mg^{2+}, Ni^{2+}, Mn^{2+}, Zn^{2+}, and Cd^{2+}) or 2 small molecules (i.e., dopamine and uric acid) in equimolar (100 μM) concentration. When H_2O_2 was present in the mixture solutions of metal ions, dopamine, or uric acid, signal change was comparable to that obtained with H_2O_2 only (red bars). On the other hand, only a minimal change was observed in the case of absence of H_2O_2 (black bars). For demonstrating the performance of the sensor, we additionally monitored H_2O_2 generation by superoxide dismutase (SOD) enzymatic reaction (Fig. S7, ESI†).

In summary, we developed a novel and sensitive method for detection of H_2O_2 using single nanoparticles and redox active Cyt *c* mediated plasmon resonance energy transfer. Using the proposed method, H_2O_2 was successfully detected at a wide range of concentration from 100 mM to 10 nM. The detection limit of the proposed method is much lower than that of the conventional optical method. Selectivity in the presence of other biologically relevant metal ions and small molecules was also achieved. We believe that the use of a single nanoparticle as a sensing probe could provide an avenue for achieving dynamic, high spatial resolution monitoring of ROS in extra- and intra-cellular environments based on the merits of this approach.

This research was supported by the Basic Science Research Program through the National Research Foundation of Korea (NRF) funded by the Ministry of Science, ICT & Future Planning (2014R1A1A1038069).

Notes and references

1 M. Giorgio, M. Trinei, E. Migliaccio and P. G. Pelicci, *Nat. Rev. Mol. Cell Biol.*, 2007, **8**, 722a-728.
2 M. Abo, Y. Urano, K. Hanaoka, T. Terai, T. Komatsu and T. Nagano, *J. Am. Chem. Soc.*, 2011, **133**, 10629-10637.
3 A. A. Karyakin, E. A. Puganova, I. A. Budashov, I. N. Kurochkin, E. E. Karyakina, V. A. Levchenko, V. N. Matveyenko and S. D. Varfolomeyev, *Anal. Chem.*, 2004, **76**, 474-478.
4 H. Cai, *Cardiovasc. Res.*, 2005, **68**, 26-36.
5 B. Halliwell, M. V. Clement and L. H. Long, *FEBS Lett.*, 2000, **486**, 10-13.
6 J. D. La Favor, E. J. Anderson and R. C. Hickner, *Physiol. Res.*, 2014, **63**, 387-392.
7 B. Halliwell, M. V. Clement, J. Ramalingam and L. H. Long, *IUBMB Life*, 2000, **50**, 251-257.
8 J. R. Stone, *Arch. Biochem. Biophys.*, 2004, **422**, 119-124.
9 R. H. Burdon, *Free Radic. Bio. Med.*, 1995, **18**, 775-794.
10 M. C. Carreras and J. J. Poderoso, *Am. J. Physiol-Cell Ph.*, 2007, **29**, C1569-C1580.
11 F. He, Y. L. Tang, M. H. Yu, S. Wang, Y. L. Li and D. B. Zhu, *Adv. Funct. Mater.*, 2006, **16**, 91-94.
12 X. Y. Shan, L. J. Chai, J. J. Ma, Z. S. Qian, J. R. Chen and H. Feng, *Analyst*, 2014, **139**, 2322-2325.
13 A. L. Hu, Y. H. Liu, H. H. Deng, G. L. Hong, A. L. Liu, X. H. Lin, X. L. Xia and W. Chen, *Biosens. Bioelectron.*, 2014, **61**, 374-378.

14 Y. C. Shiang, C. C. Huang and H. T. Chang, *Chem. Commun.*, 2009, DOI: Doi 10.1039/B901916b, 3437-3439.
15 A. R. Lippert, T. Gschneidtner and C. J. Chang, *Chem. Commun.*, 2010, **46**, 7510-7512.
16 C. A. Cohn, A. Pak, D. Strongin and M. A. Schoonen, *Geochem. T.*, 2005, **6**, 47-51.
17 E. Graf and J. T. Penniston, *Clin. Chem.*, 1980, **26**, 658-660.
18 C. W. Chuang, L. Y. Luo, M. S. Chang and J. S. Shih, *J. Chin. Chem. Soc.*, 2009, **56**, 771-777.
19 A. S. Rad, M. Jahanshahi, M. Ardjmand and A. A. Safekordi, *Int. J. Electrochem. Sci.*, 2012, **7**, 2623-2632.
20 T. Ito, M. Kunimatsu, S. Kaneko, Y. Hirabayashi, M. Soga, Y. Agawa and K. Suzuki, *Talanta*, 2012, **99**, 865-870.
21 Z. Y. Miao, D. Zhang and Q. Chen, *Materials*, 2014, **7**, 2945-2955.
22 R. Fujita, *Talanta*, 1991, **38**, 521-523.
23 V. S. Shivankar and N. V. Thakkar, *J. Sci. Ind. Res.*, 2005, **64**, 496-503.
24 B. B. Jiang, X. W. Wei, F. H. Wu, K. L. Wu, L. Chen, G. Z. Yuan, C. Dong and Y. Ye, *Microchim. Acta*, 2014, **181**, 1463-1470.
25 G. Scandurra, A. Arena, C. Ciofi and G. Saitta, *Sensors*, 2013, **13**, 3878-3888.
26 G. Su, Y. Wei and M. Guo, *Am. J. Anal. Chem.*, 2011, **02**, 879-884.
27 R. Dixit and R. Cyr, *Plant J.*, 2003, **36**, 280-290.
28 I. Choi, H. D. Song, S. Lee, Y. I. Yang, T. Kang and J. Yi, *J. Am. Chem. Soc.*, 2012, **134**, 12083-12090.
29 H. D. Song, I. Choi, S. Lee, Y. I. Yang, T. Kang and J. Yi, *Anal. Chem.*, 2013, **85**, 7980-7986.
30 J. Zhou, C. N. Liao, L. M. Zhang, Q. G. Wang and Y. Tian, *Anal. Ch...*, 2014, **86**, 4395-4401.
31 H. B. Dixon and R. McIntosh, *Nature*, 1967, **213**, 399-400.
32 G. Suarez, C. Santschi, O. J. F. Martin and V. I. Slaveykova, *Biosen... Bioelectron.*, 2013, **42**, 385-390.
33 Y. G. Zhao, Z. B. Wang and J. X. Xu, *J. Biol. Chem.*, 2003, **278**, 235...-2360.
34 J. D. Rush and W. H. Koppenol, *J. Biol. Chem.*, 1986, **261**, 6730-6733.
35 S. E. J. Bowman and K. L. Bren, *Nat. Prod. Rep.*, 2008, **25**, 1118-1130.
36 P. L. Vandewalle and N. O. Petersen, *FEBS Lett.*, 1987, **210**, 195-198.
37 G. L. Liu, Y. T. Long, Y. Choi, T. Kang and L. P. Lee, *Nat. Method* 2007, **4**, 1015-1017.
38 L. Shi, C. Jing, Z. Gu and Y. T. Long, *Sci. Rep.*, 2015, **5**, 10142.
39 Y. H. Choi, T. Kang and L. P. Lee, *Nano Lett.*, 2009, **9**, 85-90.
40 A. E. Augspurger, A. S. Stender, R. Han and N. Fang, *Anal. Chem.*, 201... **86**, 1196-1201.
41 T. Vo-Dinh, S. Dutta-Gupta, G. Suarez, C. Santschi, L. Juillerat-Jeanner..., O. J. F. Martin and J. R. Lakowicz, 2012, **8234**, 82340K:1-6.
42 S. Y. Wang, N. Kristian, S. P. Jiang and X. Wang, *Nanotechnology*, 2009, **20**.
43 H. D. Song, I. Choi, Y. I. Yang, S. Hong, S. Lee, T. Kang and J. Y..., *Nanotechnology*, 2010, **21**.
44 C. Damle, K. Biswas and M. Sastry, *Langmuir*, 2001, **17**, 7156-7159.
45 N. H. Kim, M. S. Jeong, S. Y. Choir and J. H. Kang, *Mol. Cells*, 2006, **22**, 220-227.